# Single-Molecule Microscopy Studies of Electric-Field Poling in Chromophore−Polymer Composite Materials

**Paul M. Wallace, Daniel R. B. Sluss, Larry R. Dalton, Bruce H. Robinson, and Philip J. Reid***

*Department of Chemistry, University of Washington, Box 351700, Seattle, Washington 98195*

*Received: August 18, 2005; In Final Form: October 13, 2005*

One strategy for increasing the efficiency of organic electrooptic devices based on chromophore−polymer composite materials is to improve chromophore ordering. In these materials, ordering is induced through the interaction of the chromophore dipole moment with an external electric field, applied at temperatures near the $T_g$ of the polymer host, a process referred to as "poling". To provide insight into the molecular details of the poling process under conditions representative of device construction, the rotational dynamics of single 4-dicyano-methylene-2-methyl-6-(*p*-(dimethylamino)styryl)-4H-pyran (DCM) molecules in poly(methyl acrylate) at $T = T_g + 11$ °C in the presence and absence of an electric field are investigated using single-molecule confocal fluorescence microscopy. Single-molecule rotational dynamics are monitored through the time evolution of the fluorescence anisotropy. The anisotropy correlation function demonstrates nonexponential decay, with $\beta$ values derived from fits using the Kohlrausch−Williams−Watts law ranging from 0.7 to 1 with $\langle\beta_{KWW}\rangle = 0.83$. This observation is consistent with previous studies of molecular rotation dynamics in polymer melts and reflects the dynamical heterogeneity provided by the polymer host. The rotational dynamics of DCM are weakly perturbed in the presence of a 50 V/$\mu$m electric field, typical of the field strength employed in device construction. The expected perturbation of the rotational dynamics is determined and found to be consistent with the alignment potential created by the electric field relative to the amount of thermal energy available. The relevance of these findings with respect to current models of the poling process is discussed. This work demonstrates the utility of polarization-sensitive single-molecule microscopy in elucidating the details of molecular reorientation during poling.

## Introduction

Recent advances in organic photonic materials suggest that these materials will play an important role in next generation electrooptical (EO) devices.[1−15] Organic EO devices hold the potential of higher switching frequencies and lower operational voltages when compared to current inorganic materials (i.e., $LiNO_3$). For example, polymer-based materials with electrooptic coefficients in excess of 100 pm/V and switching frequencies greater than 100 GHz have been demonstrated.[9] However, fulfilling the promise of these materials requires a molecular-level understanding of the issues that limit their efficiency.

Perhaps the central issue surrounding the development of EO materials is the translation of molecular systems with large hyperpolarizabilties, $\beta$, into macroscopic assemblies having a correspondingly large EO activity.[7,13] The EO response is one of several effects derived from the $\chi^{(2)}$ level of susceptibility.[16] Chromophore−polymer composite materials lack inherent noncentrosymmetry, which is required for finite $\chi^{(2)}$ response. In chromophore−polymer composite systems, material noncentrosymmetry is introduced through the use of an external electric field or "poling" field that induces chromophore alignment through interaction with the molecular dipole moment ($\mu$). In the typical poling process, the polymer composite is heated near the glass transition temperature ($T_g$), allowing the chromophores to reorient in response to the poling field. The composite is then cooled below $T_g$ to preserve the field-induced chromophore alignment. The EO activity is related to $\beta$ and the extent of molecular order as follows[14]

$$\mathrm{EO} \propto N\beta\langle\cos^3\theta\rangle \tag{1}$$

where $N$ is the chromophore number density and $\langle\cos^3\theta\rangle$ is the chromophore orientation parameter. Equation 1 demonstrates that one strategy for optimizing EO activity is to maximize the extent of molecular order; therefore, understanding the details of molecular reorientation in response to the poling field is a critical step toward the development of more efficient polymer-based EO devices.

Theoretical techniques have been used to explore the details of the poling process.[16−24] Consistent with simple statistical-mechanical arguments, these studies have shown that in the dilute chromophore limit the extent of molecular order is dependent on the product of the molecular dipole moment and poling field strength ($E$) versus the amount of thermal energy available, or simply $\mu E/kT$. In these studies, the field strengths investigated are generally much greater than $kT$ in contrast to experimental conditions where dielectric breakdown limits usable poling fields to ≤100 V/$\mu$m, corresponding to regimes in which $\mu E < kT$. In addition, the computational studies generally employ a gas-phase lattice model in which the environment provided by the polymer host is assumed to be homogeneous, and the interactions between the chromophore and the host matrix are ignored. The influence of polymer dynamics and the environmental heterogeneity that typifies polymer environments remain open issues with respect to poling efficacy. Clearly, experimental techniques capable of following

* Author to whom correspondence should be addressed. E-mail: preid@chem.washington.edu.

10.1021/jp0546711 CCC: $33.50 
Published on Web 12/13/2005

molecular reorientation dynamics in polymer environments especially under experimentally relevant poling conditions are required to evaluate these models and to provide further insight into the molecular details operative in the poling process.

Polarization-sensitive confocal microscopy is a technique by which to monitor the spatial orientation and rotational dynamics of single molecules.[25−36] This technique has been used to measure the rotational dynamics of rhodamine dyes in polymers at temperatures slightly above $T_g$.[27,29,31,33,34] These experiments were designed to determine the contribution of spatial and temporal homogeneity to the complex reorientational dynamics observed in polymers close to $T_g$. Nonexponential rotational correlation decay dynamics were observed consistent with environmental heterogeneity of the polymer environment. In addition, two polymers were studied at similar temperatures relative to $T_g$, and the molecular rotational dynamics were found to differ between the two polymer hosts.[29] This observation indicates that the poling temperature relative to $T_g$ may not be the only parameter that influences molecular reorientation in response to the poling field.

In this paper, we present a single-molecule confocal microscopy study of electric-field poling in a chromophore−polymer composite material. Polarization-sensitive single-molecule microscopy of the model nonlinear optical chromophore, 4-dicyano-methylene-2-methyl-6-(*p*-(dimethylamino)styryl)-4H-pyran (DCM), in poly(methyl acrylate) (PMA) at $T = T_g + 11$ °C is performed. Electric fields on the order of 50 V/$\mu$m are applied to the material, consistent with typical experimental poling conditions. The observed single-molecule rotational dynamics in the presence and absence of the electric field are analyzed to determine the change in rotational dynamics introduced by the presence of the poling field. We find that the chromophore rotational dynamics are nonexponential, consistent with previous studies of molecular rotation dynamics in polymers. In the presence of the poling field the rotational dynamics are modestly perturbed, consistent with the fact that the amount of available thermal energy is greater than the potential energy of interaction between the molecular dipole and the applied field. The relevance of these results with respect to current models of the poling process is discussed. Finally, this work demonstrates the utility of polarization-sensitive single-molecule microscopy in elucidating the details of molecular reorientation during poling.

## Experimental Section

**Coverslip Electrode Fabrication.** Coverslips outfitted with electrodes designed for poling in a geometry suitable for single-molecule microscopy were constructed as follows. Glass coverslips (Corning No. 1, 25 × 25 mm$^2$) were cleaned in a boiling solution of 3:2:1 deionized (DI) water/ammonium hydroxide/hydrogen peroxide for 1 h. After being rinsed with DI water and drying, five coverslips were bonded to a 100 mm silicon wafer using 5 $\mu$L of acetone saturated with Crystalbond (509, Aremco). The assembled wafers were allowed to dry overnight. Aluminum electrodes were deposited on 18 wafers per batch by evaporating aluminum (99.99%, Kurt J. Lesker Co., Livermore, CA) in an aluminum alloy e-beam evaporator (NRC 3117, Varian, Inc., Palo Alto, CA) until a film thickness of 1.5 $\mu$m was achieved. This electrode height relative to the microscope depth of field ensured that the imaged molecules experience a uniform electric field. Patterning of the electrodes was accomplished by conventional positive photolithography. Photoresist (AZ 1512, AZ Electronic Materials, Somerville, NJ) was deposited to a thickness of ~1.2 $\mu$m and soft-baked at 100 °C for 3 min. The wafers were then exposed to 38.25 mJ/cm$^2$ of 362 nm light (AB-M, Inc., Silicon Valley, CA) through a chrome-on-glass mask (Photo Sciences, Inc., Torrance, CA), providing for electrode gaps of 5, 10, and 20 $\mu$m as shown in Figure 1. A solution of AZ 351 diluted 1:4 with deionized water was used to develop the wafers for 40 s after which the wafers were rinsed. The wafers were then submerged in a bath of aluminum etch with surfactant (Ashland, Inc., Columbus, OH) heated to 65 °C for 60 s and rinsed. Removal of residual photoresist was performed using a bath of AZ300T warmed to 65 °C. The wafers were then rinsed and dried with a stream of nitrogen gas. To ensure coverslip cleanliness suitable for single-molecule studies, the wafers were postprocessed with an additional UV exposure of 6 mJ/cm$^2$ of 362 nm light to soften any residual photoresist. The electrodes were separated from the silicon wafers by soaking in acetone with sonication for approximately 15 min, rinsing, and drying. Finally, the electrodes were subjected to a final cleaning bath of AZ300T heated to about 100 °C for 20 min followed by a final rinse and drying.

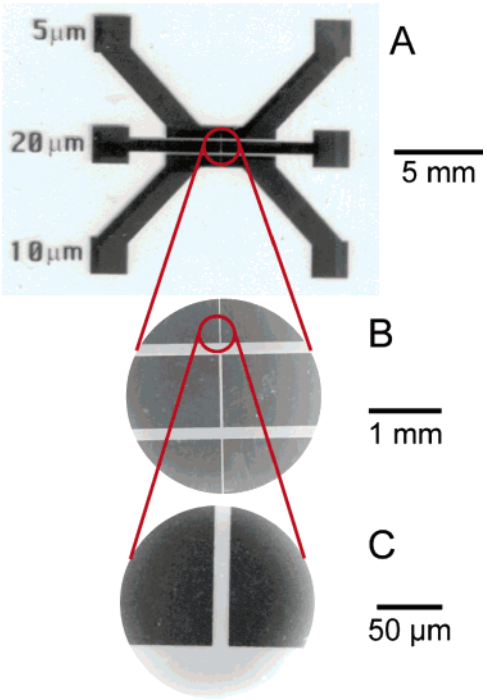


**Figure 1.** (A) Full view of the electrode, (B) magnified 20× with measured gaps of 12.4, 28.0, and 17.2 $\mu$m, and (C) 100× detail of the 12.4 $\mu$m gap.

**Sample Preparation.** The laser dye 4-dicyano-methylene-2-methyl-6-(*p*-(dimethylamino)styryl)-4H-pyran (DCM, Aldrich, 98%) was used as received. DCM was selected for these studies because it is a model nonlinear optical chromophore, possesses an appreciable dipole moment of 10.2 ± 0.1 D,[37] and demonstrates a fluorescence quantum yield of 0.78 in poly(methyl methacrylate).[38] Stock solutions of 4 × $10^{-9}$ M DCM in cyclopentanone (Aldrich, ≥99%) and 20 wt % PMA (Aldrich, molecular weight ≈ 40 kDa, $T_g$ = 303 K) in cyclopentanone were prepared and filtered (Whatman, 0.45 $\mu$m) after mixing for 24 h. Structures of both compounds are presented in Figure 2. Prior to spin-coating, the DCM and polymer solutions were mixed in a 1:4 ratio, resulting in a final concentration of 1 × $10^{-9}$ M in 15 wt % polymer solution. This concentration provided for a molecular number density consistent with single-molecule resolution. A 100 $\mu$L aliquot of this sample solution was injected on an electrode spinning at 3000 rpm for 30 s, and the resulting film thickness (200 nm) was measured by surface profilemetry (Dektak 3030).

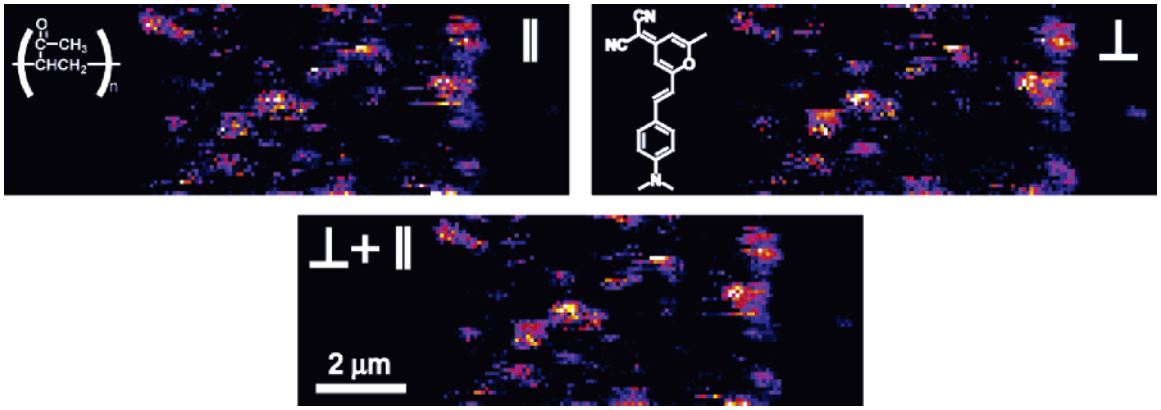


**Figure 2.** False-color images of the fluorescence from single DCM molecules. The figure presents a 15 × 5 $\mu m^2$ scan employing 0.1 $\mu$m steps of $10^{-9}$ M DCM in 15 wt % PMA. The fluorescence is polarized parallel to the applied electric field (above left) or perpendicular (above right). The color scale corresponds to counts of 50−300 per 100 ms time window. Molecular structures of PMA (left) and DCM (right) are shown. Total fluorescence is shown below with the color scale corresponding to 100−600 counts per 100 ms.

**Single-Molecule Confocal Microscopy.** Single-molecule microscopy studies were preformed using an inverted scanning fluorescence confocal microscope (Nikon T2000U).[39] Photoexcitation at 532 nm was provided by a Nd:$VO_4$ laser (Spectra-Physics Millennia). Excitation powers of ≤10 $\mu$W were employed, and the polarization of the excitation field was circularly polarized using a $\lambda/4$ waveplate. The excitation field was reflected toward the sample using a dichroic beam splitter (Chroma, z532rdc) and focused using an oil-immersion objective (Nikon, 100×, 1.3 NA). Molecular fluorescence was collected in an epi-geometry, passed through a dichroic beam splitter and through appropriate band-pass filters to isolate the fluorescence (Chroma). Spatial rejection of signal from outside the focal volume was accomplished by a 75 $\mu$m diameter pinhole. Images were acquired by scanning the sample using a closed-loop piezoelectric scan stage (Queensgate, NPS-XY-100B) with step sizes of 100 nm in both *x*- and *y*-directions. Detection of the polarized components of the fluorescence was performed using a polarizing beam splitter and a pair of single-photon-counting avalanche photodiodes (PerkinElmer, SPCM-AQR-16). The fluorescence from dye-doped polystyrene spheres (Molecular Probes) was measured daily to allow for normalization of the detector efficiencies and to optimize the resolution of the microscope. The scan stage and detector electronics were controlled using a custom Labview program. The external applied electric field was generated through the electrodes with a high-voltage power supply. All of the data was collected at an ambient room temperature of 20 ± 1 °C.

## Results

**Single-Molecule Emission.** In this study, the influence of an applied electric field on molecular orientation is measured by monitoring the fluorescence dichroism of single molecules. However, it is well-known that the high-NA objectives employed in single-molecule studies mix the polarization components of the fluorescence. Therefore, the effect of the objective on the measured dichroism must be considered. In this study the excitation field is circularly polarized such that all transition dipole orientations in the *xy*-plane of the microscope are excited. The objective collects the molecular fluorescence and relays this emission a polarizing beam splitter that separates it into its dichroic components. To determine the effect of the high-NA objective on the measured dichroic components of the emission, we consider a single molecule where the three components of its transition dipole moment are defined as a vector in the laboratory frame

$$\hat{\mu} = \begin{pmatrix} \mu_x \\ \mu_x \\ \mu_x \end{pmatrix} \tag{2}$$

We restrict ourselves to molecules for which the absorption and emission dipole moments are coincident, an adequate assumption for the fluorophore employed in this study.[5,38] From Axelrod, who has defined the transformation between the emission from a single molecule at the image plane of a microscope and the intensity of the detected emission in the object plane where polarization discrimination occurs, the optical coordinate system is defined as a right-hand frame with the $X_3$-axis parallel to the optical axes of the microscope and the $X_1$-axis parallel to the applied electric field.[40] The fluorescence propagates toward the objective in a direction defined by the polar angle, $\sigma$, relative to $X_1$ and an azimuthal angle, $\phi$, relative to $X_3$. An infinity-corrected objective is employed in this study; therefore, the rays captured by the objective are refracted and made to be parallel to $X_3$. The transformation is described as a series of rotations of $-\phi$ about $X_1$, $-\sigma$ about the new $X_2$, and $+\phi$ about the new $X_1$ resulting in the following rotation matrix

$$R(\sigma,\phi) = \begin{pmatrix} \cos\sigma\cos^2\phi + \sin^2\phi & \cos\phi\sin\phi(1-\cos\sigma) & -\cos\phi\sin\sigma \\ \cos\phi\sin\phi(1-\cos\sigma) & \cos^2\phi + \cos\sigma\sin^2\phi & \sin\phi\sin\sigma \\ \cos\phi\sin\sigma & -\sin\phi\sin\sigma & \cos\sigma \end{pmatrix} \tag{3}$$

With this rotation matrix, the molecular transition dipole in the object plane of the microscope where polarization discrimination of the emission occurs is defined as

$$\hat{\mu}(\sigma,\phi) = R(\sigma,\phi)\cdot\hat{\mu} \tag{4}$$

The observed polarized fluorescence intensity, $I_{\parallel,\perp}$, is related to the square of the transition dipole moment as projected onto the object plane as follows

$$I_{\parallel,\perp}(\Omega) = \int_{\sigma=0}^{\theta_{obj}} \int_{\phi=0}^{2\pi} (\hat{\mu}(\sigma,\phi))^2 \sin\sigma \, d\sigma \, d\phi \tag{5}$$

In eq 5, the integral over $\sigma$ is limited by the angle subtended by the objective ($\theta_{obj}$) defined by the NA of the objective

according to NA = $n(\sin\theta_{obj})$. Evaluation of eq 5 is accomplished using eqs 3 and 4, resulting in the following expressions for $I_{||}$ and $I_{\perp}$

$$I_{||} = K_1\mu_x^2 + K_2\mu_y^2 + K_3\mu_z^2$$
$$I_{\perp} = K_2\mu_x^2 + K_1\mu_y^2 + K_3\mu_z^2 \quad (6)$$

In eq 6, $K_1$, $K_2$, and $K_3$ define the extent of emission polarization mixing defined by the NA of the objective employed. In this work, a 1.3 NA oil-immersion objective ($n = 1.518$) dictates that $\theta_{obj} = 59°$. With this angle, $K_1$, $K_2$, and $K_3$ are equal to

$$K_1 = \frac{1}{4}(5 - 3\cos\theta_{obj} - \cos^2\theta_{obj} - \cos^3\theta_{obj}) = 2.393$$
$$K_2 = \frac{1}{12}(1 - 3\cos\theta_{obj} + 3\cos^2\theta_{obj} - \cos^3\theta_{obj}) = 0.0296$$
$$K_3 = \frac{1}{3}(2 - 3\cos\theta_{obj} + \cos^3\theta_{obj}) = 0.616 \quad (7)$$

Recasting eq 6 in a matrix form, we make the following definitions

$$\hat{I} = \begin{pmatrix} I_{||} \\ I_{\perp} \end{pmatrix} \quad \hat{\epsilon} = \begin{pmatrix} 1 \\ 1 \end{pmatrix} \quad \underset{\sim}{K} = \begin{pmatrix} K_1 & K_2 \\ K_2 & K_1 \end{pmatrix}$$

With these definitions eq 6 becomes

$$\hat{I} = \underset{\sim}{K}\begin{pmatrix} \mu_x^2 \\ \mu_y^2 \end{pmatrix} + K_3\hat{\epsilon}\mu_z^2 \quad (8)$$

As pointed out above, the transition dipole moment is expressed in the frame of the optical system. This frame may be related to the molecular frame by a standard Euler rotation

$$\hat{\mu} = R(\Omega)\begin{pmatrix} 0 \\ 0 \\ |\mu_o| \end{pmatrix} = |\mu_o|\begin{pmatrix} \sin\theta\cos\varphi \\ \sin\theta\sin\varphi \\ \cos\theta \end{pmatrix} \quad (9)$$

The definition of $\hat{\mu}$ provided by eq 9 is then related to the fluorescence intensity in terms of the rotation angles defining the orientation of the transition dipole in the molecular frame

$$\hat{I} = |\mu_o|^2\left\{\sin^2\theta\underset{\sim}{K}\begin{pmatrix} \cos\varphi^2 \\ \sin\varphi^2 \end{pmatrix} + K_3\hat{\epsilon}\cos^2\theta\right\} \quad (10)$$

The matrix equation can be simplified by using the $K_{\%}$ matrix to transform the intensities in an effort to partially undo the polarization mixing introduced by the objective

$$\hat{\mathscr{T}} = \underset{\sim}{K}^{-1}\hat{I} = |\mu_o|^2\left\{\sin^2\theta\begin{pmatrix} \cos\varphi^2 \\ \sin\varphi^2 \end{pmatrix} + \kappa\hat{\epsilon}\cos^2\theta\right\} \quad (11)$$

where $K_{\%}^{-1}$ and $\kappa$ are equal to

$$\underset{\sim}{K}^{-1} = \frac{1}{K_1^2 - K_2^2}\begin{pmatrix} K_1 & -K_2 \\ -K_2 & K_1 \end{pmatrix} \quad \kappa = \frac{K_3}{K_1 + K_2}$$

The new intensities, $\bar{\mathscr{T}}$, may be considered to be partially back-transformed from the object frame to the molecular frame. The correction factor, $\kappa = 0.229$ for the present case, represents the extent to which this approach does not fully remove the effects of the large NA objective. However, taking the difference between the back-transformed parallel and perpendicular intensities has the effect of removing this correction. The sum of the two polarization components of the emission will contain the correction but will not demonstrate any dependence on the minor Euler angle.

$$|\mu_o|^{-2}(\mathscr{T}_{||} - \mathscr{T}_{\perp}) = \sin^2\theta(\cos^2\varphi - \sin^2\varphi) = \sin^2\theta\cos 2\varphi$$
$$|\mu_o|^{-2}(\mathscr{T}_{||} + \mathscr{T}_{\perp}) = \sin^2\theta + 2\kappa\cos^2\theta \quad (12)$$

Although our focus has been on the fluorescence from a single molecule, if more than one molecule contributes to the observed fluorescence intensity, then the right-hand side of eq 12 could be modified to account for multiple fluorophores by summing over the angles of each of the individual molecules that are within the focus of the beam. In the dilute limit, where coupling of the chromophore transitions moments can be ignored, the magnitude of the transition dipole of each molecule is a constant. An identical result will be obtained for a single-molecule experiment where individual contributions are acquired and summed to recreate the ensemble value. In either case, with the equilibrium probability distribution as a function of the angles, $P_{eq}(\theta,\varphi)$, eq 12 would become

$$|\mu_o|^{-2}\langle(\mathscr{T}_{||} - \mathscr{T}_{\perp})\rangle = \langle\sin^2\theta\cos 2\varphi\rangle$$
$$|\mu_o|^{-2}\langle(\mathscr{T}_{||} + \mathscr{T}_{\perp})\rangle = \langle\sin^2\theta + 2\kappa\cos^2\theta\rangle \quad (13)$$

In the poling process, the presence of an electric field is expected to bias the molecular orientation distribution toward the direction of the electric field. The magnitude of this interaction is dependent on both the magnitude of the molecular dipole moment and the applied field. The molecule of interest in this study, DCM, possesses a dipole moment of ~10 D, and fields of 50 V/$\mu$m are employed. The field is parallel to the $X_1$-axis of the optical system; therefore, the equilibrium probability distribution is no longer uniform over all orientations. The orientational distribution will be governed by the Boltzmann probability distribution

$$P_{eq}(\theta,\varphi) = \frac{e^{f\cos\varphi}}{\int_\theta\int_\varphi e^{f\cos\varphi}\sin\theta\,d\theta\,d\varphi} \quad (14)$$

In eq 14, $f$ is equal to $\mu E/kT$ where $\mu$ is the magnitude of the molecular dipole moment, $E$ is the magnitude of the poling field, $k$ is Boltzmann's constant, and $T$ is temperature. For the experimental conditions of this study

$$f = \frac{\mu E}{kT} \approx 0.4$$

Internal field factors are ignored in this expression. Through the use of eqs 13 and 14, the effect of the poling field on the bulk averaged dichroism is given by

$$|\mu_o|^{-2}\langle(\mathscr{T}_{||} - \mathscr{T}_{\perp})\rangle = \langle\sin^2\theta(\cos^2\varphi - \sin^2\varphi)\rangle = \frac{1}{2}\langle\cos 2\varphi\rangle$$
$$|\mu_o|^{-2}\langle(\mathscr{T}_{||} + \mathscr{T}_{\perp})\rangle = \langle\sin^2\theta + 2\kappa\cos^2\theta\rangle = \frac{1}{2}(1 + 2\kappa)$$
$$\langle\cos 2\varphi\rangle = \frac{\int_{\varphi=0}^{2\pi}\cos 2\varphi\, e^{f\cos\varphi}\,d\varphi}{\int_{\varphi=0}^{2\pi} e^{f\cos\varphi}\,d\varphi} \quad (15)$$

And the integral in eq 15 can be written in terms of Bessel functions as follows

$$J_0(-if) = \frac{1}{\pi}\int_0^{\pi} e^{f\cos\varphi}\, d\varphi$$

$$J_2(-if) = \frac{-1}{\pi}\int_0^{\pi} \cos(2\varphi)\, e^{f\cos\varphi}\, d\varphi$$

$$\langle(\cos^2\varphi - \sin^2\varphi)\rangle = \frac{-J_2(-if)}{J_0(-if)} = 0.015 \approx \frac{1}{8}f^2 \quad (16)$$

We will make use of this final result below when describing the observed variation in the fluorescence dichroism with the application of the poling field.

**Reduced Linear Dichroism.** As demonstrated in previous studies of chromophores in polymer melts, the rotational dynamics of the chromophore can be described through the time evolution of the emission dichroism expressed as the reduced dichroism, $A(t)$ [27]

$$A_I(t) = \frac{I_{||}(t) - I_{\perp}(t)}{I_{||}(t) + I_{\perp}(t)} \quad (17)$$

Alternative expressions to eq 17 have been developed.[5] Rather than evaluate the anisotropy ratio in terms of the raw intensity values, a more fundamental approach is to evaluate an anisotropy ratio in terms of the back-transformed intensities. Therefore, we can define a different form as

$$A_{\mathscr{T}}(t) = \frac{\mathscr{T}_{||}(t) - \mathscr{T}_{\perp}(t)}{\mathscr{T}_{||}(t) + \mathscr{T}_{\perp}(t)} \quad (18)$$

For a single molecule, the above expression has the advantage of being closely related to the orientation parameters. Using the above definitions, we find

$$A_{\mathscr{T}}(t) = \frac{\mathscr{T}_{||}(t) - \mathscr{T}_{\perp}(t)}{\mathscr{T}_{||}(t) + \mathscr{T}_{\perp}(t)} = \cos 2\varphi \frac{\sin^2\theta}{\sin^2\theta + 2\kappa\cos^2\theta} = \cos 2\varphi \frac{1}{1 + 2\kappa\cot^2\theta} \quad (19)$$

As the orientation of the molecule changes in time, the anisotropy ratio will evolve in time. This form of the anisotropy is nearly the same as that of $\cos 2\varphi$, with the correction factor scaled by the parameter $\kappa$, which is a function of the objective NA. The rotational dynamics as reflected by $A(t)$ can be quantified by the autocorrelation of this quantity, defined as $C(t)$, which is calculated as follows

$$C(t) = \frac{\sum_{t=0}^{T} A(0)A(0+t)}{|A(0)|^2} \quad (20)$$

where $A(t)$ can be determined using $A_I(t)$ or $A_{\mathscr{T}}(t)$. The temporal behavior of $C(t)$ demonstrates nonexponential decay; therefore, the temporal evolution of this function generally is fit using the Kholrausch−William−Watts (KWW) stretched exponential function[27,41]

$$C(t) = \exp[-(t/\tau_{KWW})^{\beta}] \quad (21)$$

In eq 21, $\tau_{KWW}$ is the apparent decay constant, and $\beta$ can range from 0 to 1 with $\beta = 1$ representing the single-exponential decay expected for Brownian rotational diffusion. We will refer to $\beta$ as $\beta_{KWW}$ throughout the text to avoid confusion with the molecular hyperpolarizability. The weighted average time scale, $\tau_c$, produces a measure of the single-molecule rotation times and is related to $C(t)$ as follows

$$\tau_c = \int_0^{\infty} C(t)\, dt = \frac{\tau_{KWW}}{\beta}\Gamma\left(\frac{1}{\beta}\right) \quad (22)$$

Finally, the ensemble-averaged correlation time, $\langle\tau_c\rangle$, is calculated from the distribution of weighted average times as follows

$$\langle\tau_c\rangle = \frac{1}{N}\sum_{i=1}^{N}(\tau_c)_i \quad (23)$$

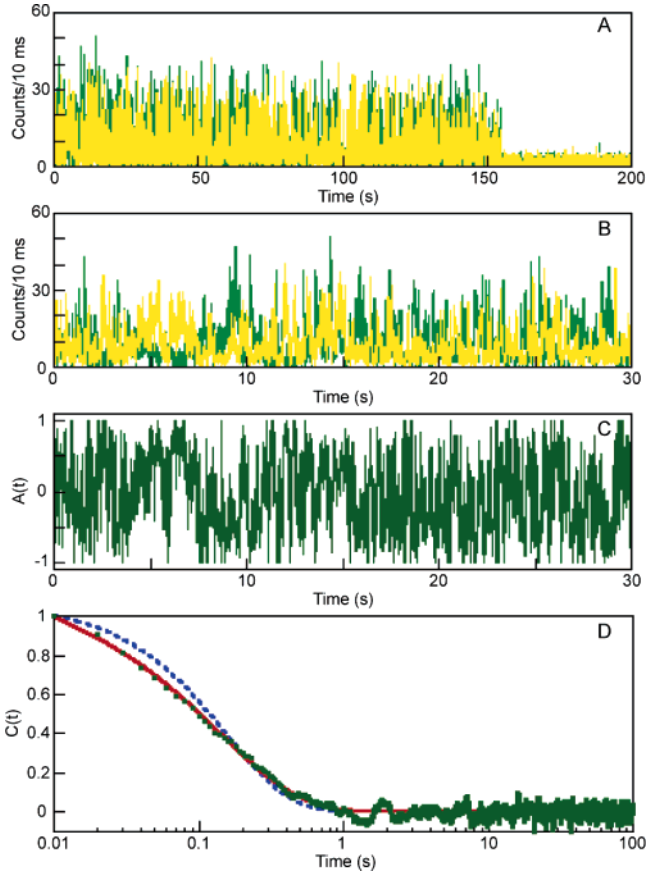


**Figure 3.** Typical single-molecule time trace of DCM in PMA ($T_g$ + 11 °C). Part A presents the signal for the two dichroic components of the fluorescence (|| to gap as yellow, ⊥ as green). A single-step bleach at 150 s is observed, consistent with single-molecule photodestruction. In part B, the first 30 s of the evolution in part A is shown to more clearly depict the rotational dynamics. The reduced linear dichroism, $A(t)$, is illustrated in part C. Part D is a fit to the autocorrelation of the transient showing both an exponential fit (dashed, $\tau = 0.16$) and a fit to the Kohlrausch−Williams−Watts law (solid, $\tau_{KWW} = 0.15$ and $\beta_{KWW} = 0.79$).

**Single-Molecule Microscopy Results.** A 15 × 5 $\mu$m$^2$ image of the fluorescence from single DCM molecules located between electrodes separated by 10 $\mu$m is presented in Figure 2. The spots corresponding to emission from single molecules demonstrate intensity fluctuations from one pixel to the next, reflecting single-molecule rotational dynamics that occur on the time scale of data collection. The analysis required to connect the fluorescence intensity data to the molecular rotation dynamics is schematically illustrated in Figure 3. In a given experiment,

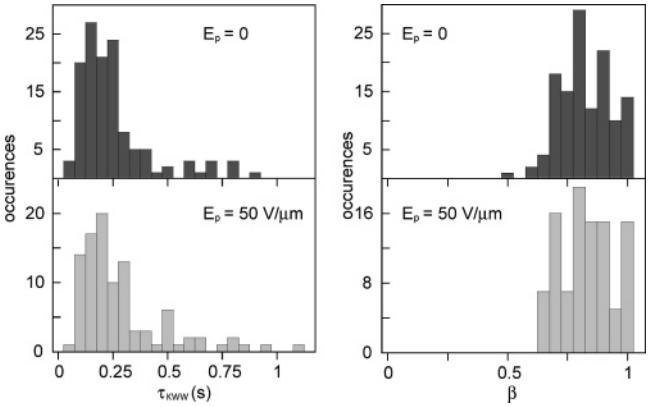


**Figure 4.** Histograms of fit parameters $\tau_{KWW}$ (left) and $\beta_{KWW}$ (right). The values with no applied field are shown at the top, and at the bottom are values in the presence of a 50 ± 5 V/$\mu$m electric field.

single molecules were located by performing a raster scan within the electrode's gap until the measured intensity from both channels exceeded a preset threshold value. When this threshold was exceeded, scanning was paused, and the intensity on both detectors was monitored as a function of time for up to 200 s. Figure 3A presents $I_{||}(t)$ and $I_{\perp}(t)$ measured for a representative threshold event. Fluctuations in intensities between the polarization components are observed due to molecular rotation until permanent loss of signal occurs due to photodestruction. Figure 3B is an expanded view of the first 30 s of the data shown in Figure 3A, and anticorrelation of the observed intensities is evident, consistent with molecular rotation. Through the use of $I_{||}$ and $I_{\perp}$, $A(t)$ is calculated as described by eq 17, with the particular $A(t)$ calculated from the data in Figure 3B shown in Figure 3C. The autocorrelation of $A(t)$ before the photodestruction event, $C(t)$, is shown in Figure 3D. Consistent with previous studies of molecular rotational dynamics in polymer melts, the decay of $C(t)$ is not exponential as illustrated by the mismatch between the exponential fit (dashed line) and the data (green squares). In contrast, the data are better fit by the stretched exponential function (solid line) with $\tau_{KWW} = 0.15$ s and $\beta_{KWW} = 0.79$. For molecules in the absence of the poling field, $\tau_{KWW}$ was found to vary between 0.05 and 0.89 s with $\langle\tau_{KWW}\rangle = 0.25 \pm 0.02$ s, and values of $\beta_{KWW}$ ranged between 0.5 and 1 with $\langle\beta_{KWW}\rangle = 0.83 \pm 0.01$. Histograms of $\tau_{KWW}$ and $\beta_{KWW}$ in the presence and absence of the poling field are presented in Figure 4. The deviation of $\beta_{KWW}$ from 1 suggests that the rotational dynamics are reflecting the heterogeneous environment provided by the polymer host; however, the preponderance of values lie between 0.7 and 1, demonstrating that the rotational dynamics are near-exponential. Furthermore, if the data presented in Figure 3 are combined such that the time spacings are every 100 ms, the vast majority of *C(t)* functions demonstrate exponential decay.

The effect of an applied electric field on the rotational dynamics ($\tau_c$) was determined by comparing the weighted average correlation times as calculated in eq 22 for molecules in the presence and absence of the poling field. Figure 5 presents the values of $\tau_c$ determined for 99 molecules in the absence of an applied external field and for 120 molecules in the presence of a 50 V/$\mu$m field. Although the histograms with and without the external field are similar, a shift to higher $\tau_c$ values is observed in the presence of the poling field. This slight enhancement in $\tau_c$ is reflected by the average correlation times ($\langle\tau_c\rangle$) of 0.29 ± 0.02 and 0.33 ± 0.03 s in the absence and presence of the electric field, respectively.

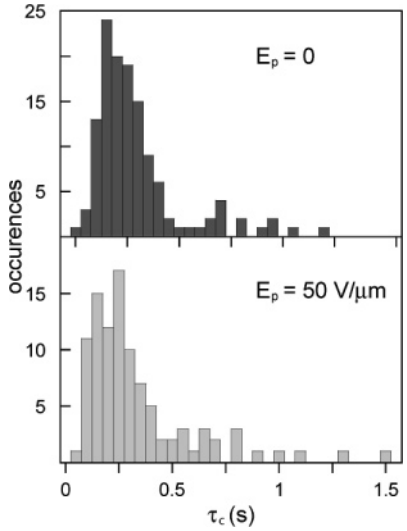


**Figure 5.** Histograms of single-molecule correlation time, $\tau_c$. The values in the absence of an applied field are shown on top, and at the bottom are values in the presence of a 50 ± 5 V/$\mu$m electric field.

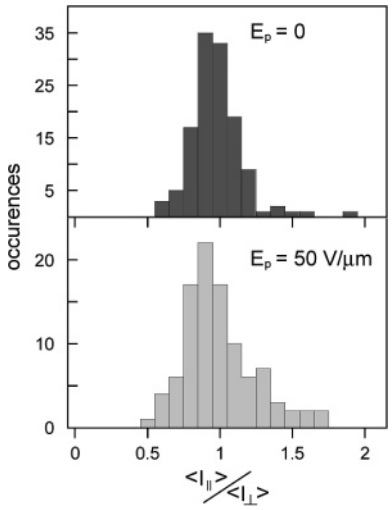


**Figure 6.** Histograms of $\langle I_P\rangle/\langle I_{\perp}\rangle$ with no applied field (top) and in the presence of a 50 ± 5 V/$\mu$m electric field (bottom).

An alternate way to gauge the effect of an applied field is illustrated in Figure 6. Here, histograms of the ratio of $I_{||}$ to $I_{\perp}$ averaged over the molecule's lifetime are shown in the presence and absence of the electric field. The application of the poling field is expected to bias the molecular alignment in the direction of the field; therefore, this should be reflected by an increase in the dichroic ratio in the presence of the electric field. The intensity ratios are 0.98 ± 0.02 with no external field, and in the presence of a 50 V/$\mu$m field the ratio undergoes a sight increase to 1.00 ± 0.03. In addition, the histogram in the presence of the electric field demonstrates broadening and skewing of the intensity ratio to values greater than unity, consistent with a biasing of the molecular orientation in the direction of the electric field.

## Discussion

**Rotational Dynamics.** The distribution of $\tau_c$ presented in Figure 5 is consistent with the heterogeneous environment of the polymer causing variation in molecular rotational dynamics between individual probe molecules. This finding is consistent with prior studies of the rotational dynamics of rhodamine dyes in PMA where a substantial variation in $\tau_c$ was also ob-

served.[27−29,31] Although distributions in $\tau_c$ are observed in all studies, there are two significant differences that should be noted. First, $\langle\tau_c\rangle$ for DCM in PMA is significantly smaller (~300 ms) than the corresponding values for the rhodamine dyes (1−50 s). The previous studies also found that $C(t)$ demonstrated significantly greater nonexponential decay, a finding that contrasts with the near-exponential decay observed here as reflected by the modest variation in $\beta_{KWW}$ and $\langle\beta_{KWW}\rangle = 0.83$ (Figure 4). One potential explanation for these differences is that the structure and electrostatic properties of DCM and rhodamine dyes are quite different. Rhodamine dyes are charged and have an approximately oblate geometry. In contrast, DCM is dipolar and has a prolate geometry. Rotational correlation times have been shown to vary for different probe molecules in the same polymer.[42] Therefore, differences in probe molecule geometry or alteration of the dielectric interaction with the polymer host may be responsible for the differences observed in these studies.

Given that the differences in $\tau_c$ may be due to structural differences between DCM and rhodamine dyes, why should the rotational correlation decay of DCM in PMA be near-exponential while rhodamine dyes demonstrate significantly more nonexponential behavior? Wang and Richert have recently demonstrated that for probe molecules in glass-forming liquids, if the rotational time constant of the probe is significantly greater than the structural relaxation time of the surrounding environment, then the rotational dynamics of the probe as reflected by decay of the linear anisotropy will demonstrate exponential decay. In this case, the observation of exponential decay is due to the rotational correlation function, reflecting the average environment experienced by the probe.[43] Although only a few measurements of the dielectric relaxation in PMA exist, the relaxation near the glass transition temperature as described within the Kohlrausch−Williams−Watts law is consistent with an average relaxation time of 0.15 s.[44] Since the temperature employed in this study is above $T_g$, the relaxation time for the polymer will presumably be on a shorter time scale. Given this, the near-exponential decay of the rotational correlation observed here may reflect the rapid fluctuations of the polymer host relative to the slower rotational dynamics of the probe.

**Poling Effects on Chromophore Orientation.** The results presented here demonstrate that at the temperature employed in this study, DCM molecules in PMA experience significant rotational mobility. This behavior is consistent with the expected enhanced rotational mobility when $T > T_g$.[33,45−48] As shown in Figures 5 and 6, the relative similarity of $\langle\tau_c\rangle$ and $\langle I_{||}\rangle/\langle I_\perp\rangle$ in the presence and absence of the poling field demonstrates that the molecular rotational dynamics of DCM are only slightly perturbed by the presence of the electric field. This observation could be viewed as surprising within the context of current conceptual descriptions of the poling process. These descriptions are largely derived from theoretical studies that have predicted significant field-induced molecular order for poling fields in excess of 100 V/$\mu$m.[13,16,18−24] However, the poling field used in this study, 50 V/$\mu$m, is representative of typical fields employed in device construction. Given a poling field of this magnitude and the dipole moment of DCM (10 D), $\mu E$ is approximately equal to $0.4kT$. Therefore, the amount of thermal energy available to DCM is significantly greater than the electrostatic potential energy created by the poling field. This energetic comparison is consistent with the observation that the poling field provides only a modest perturbation to the rotational dynamics of DCM.

The extent of the electric-field perturbation of molecular orientation can be placed in more quantitative terms. The intensity ratio distributions presented in Figure 6 demonstrate a slight alteration in the presence of the poling field. For an isotropic medium in the absence of an electric field, the time-averaged value, $\langle I_{||}\rangle/\langle I_\perp\rangle$ or more precisely $\langle\mathcal{T}_{||}\rangle/\langle\mathcal{T}_\perp\rangle$, should be unity. With the application of a poling field, molecular orientation in the direction of the field will be favored, and the ratio should become greater than unity. Through the use of eqs 11, 15, and 16, the effect of the poling field on molecular orientation as reflected by the fluorescence polarization intensity ratio expressed in terms of $f$ is

$$\frac{\langle\mathcal{T}_{||}\rangle}{\langle\mathcal{T}_\perp\rangle} = \frac{1 + 2\kappa + \frac{1}{8}f^2}{1 + 2\kappa - \frac{1}{8}f^2} \tag{24}$$

In the experiments performed here, DCM experiences a poling field of 50 V/$\mu$m such that $f \approx 0.4$, and from eq 24 a slight 2% increase in the intensity ratio is expected in the presence of the poling field. An increase of this magnitude is consistent with the data presented in Figure 6. This simple analysis demonstrates that many more single molecules would need to be interrogated to definitively measure an intensity ratio shift of this size. This behavior is largely due to the fact that linear dichroism is an even function of the molecular orientation parameter (i.e., $\cos^2\varphi$) such that linear dependence on $f$ vanishes in eq 16 by symmetry, leaving $f^2$ as the lowest-order field dependence reflected by this measurement. In contrast, $\chi^{(2)}$ techniques such as second-harmonic generation are dependent on odd functions of molecular orientation (i.e., $\cos^3\varphi$) such that linear $f$ dependence is reflected by these techniques, thereby providing a more sensitive measure of orientation for modest values of the poling field and molecular dipole moment.

The results presented here suggest that understanding the interplay between the changes in rotational dynamics accompanying a change in $T$ relative to $T_g$ of the polymer host and the strength of the applied field is critical to understanding the efficacy of poling. This is an important issue with respect to EO device construction. Specifically, EO devices generally employ electrodes in a "sandwich" geometry in which the chromophore−polymer composite is placed between an indium−tin-oxide-coated glass substrate and a metal electrode deposited on top of the composite. In poling these devices, temperatures above $T_g$ are not employed due to the mechanical stability of the electrode on top of the polymer composite; therefore, poling occurs in an environment where molecular rotational motion should be hindered. However, a handful of studies have suggested that even in polymers well below $T_g$ a subset of the chromophores experience local environments that allow for reorientation in response to the poling field. For example, the poling field response of DCM in poly(methyl methacrylate) (PMMA, $T_g = 120$ °C) has been studied by polarization-dependent two-photon fluorescence microscopy, and a slight increase in fluorescence polarized in the direction of the applied electric field was observed.[49] Other studies have also observed significant chromophore relaxation in high $T_g$ polymers well below the glass transition temperature.[50] Finally, single-molecule microscopy studies of chromophores embedded in PMMA observed that a portion of the chromophore population was mobile at temperatures well below $T_g$.[34] These results suggest that understanding the effect of the poling field on molecular orientation as the temperature is varied relative to the $T_g$ of the polymer host is needed to further define the physics underlying the poling process.

**Acknowledgment.** The National Science Foundation is acknowledged for their support of this work through the Science and Technology Center for Materials and Devices for Information Technology Research (DMR 0120967). P.J.R. is an Alfred P. Sloan Fellow and is a Cottrell Scholar of the Research Corporation. The authors thank An-Shyang "Hopper" Chu and the Washington Technology Center for assistance with microfabrication of the coverslip electrodes. The authors thank Mark Ediger (University of Wisconsin) and David Vanden Bout (University of Texas) for their advice and suggestions.

## References and Notes

(1) Burland, D.; Miller, R.; Walsh, C. *Chem. Rev.* **1994**, *94*, 31.
(2) Marder, S.; Kippelen, B.; Jen, A.; Peyambarian, N. *Nature* **1997**, *338*, 845.
(3) Chen, D.; Fetterman, H.; Chen, A.; Steier, W.; Dalton, L.; Wang, W.; Shi, Y. *Appl. Phys. Lett.* **1997**, *70*, 3335.
(4) Chen, A.; Chuyanov, V.; Zhang, H.; Garner, S.; Lee, S.; Steier, W.; Chen, J.; Wang, F.; Zhu, J.; He, M.; Ra, Y.; Mao, S.; Harper, A.; Dalton, L.; Fetterman, H. *Opt. Eng.* **1999**, *38*, 2000.
(5) Dalton, L.; Harper, A.; Ren, A.; Wang, F.; Todorova, G.; Chen, J.; Zhang, C.; Lee, M. *Ind. Eng. Chem Res.* **1999**, *38*, 8.
(6) Harper, A.; Sun, S.; Dalton, L.; Garner, S.; Chen, A.; Kalluri, S.; Steier, W.; Robinson, B. *J. Opt. Soc. Am. B* **1998**, *15*, 329.
(7) Robinson, B.; Dalton, L.; Harper, A.; Ren, A.; Wang, F.; Zhang, C.; Todorova, G.; Lee, M.; Aniszfeld, R.; Garner, S.; Chen, A.; Steier, W.; Houbrecht, S.; Persoons, A.; Ledoux, I.; Zyss, J.; Jen, A. *Chem. Phys.* **1999**, *245*, 35.
(8) Dalton, L. Nonlinear Optical Polymeric Materials: From Chromophore Design to Commercial Applications. In *Polymers for Photonics Applications I*; Advances in Polymer Science 158; Springer-Verlag: Berlin, 2002; pp 1−86.
(9) Firestone, K.; Reid, P.; Lawson, R.; Jang, S.; Dalton, L. *Inorg. Chim. Acta* **2004**, *357*, 3957.
(10) Spangler, C.; He, M.; Nickel, E.; Laquindanum, J.; Dalton, L.; Tang, N.; Hellwarth, R. *Mol. Cryst. Liq. Cryst. Sci. Technol., Sect. A* **1994**, *240*, 17.
(11) Spangler, C. W.; He, M.; Liu, P. K.; Nickel, E. G.; Laquindanum, J.; Dalton, L. R. *Nonlinear Opt.* **1995**, *10*, 147.
(12) Wang, W.; Chen, D.; Fetterman, H.; Shi, Y.; Steier, W.; Dalton, L.; Chow, P. *Appl. Phys. Lett.* **1995**, *67*, 1806.
(13) Shi, Y.; Zhang, C.; Zhang, H.; Bechtel, J.; Dalton, L.; Robinson, B.; Steier, W. *Science* **2000**, *288*, 119.
(14) Prasad, P. N.; Williams, D. J. *Introduction to Nonlinear Optical Effects in Molecules and Polymers*; John Wiley & Sons: New York, 1991.
(15) Galvan-Gonzalez, A.; Stegeman, G.; Jen, A.; Wu, X.; Canva, M.; Kowalczyk, A.; Zhang, X.; Lackritz, H.; Marder, S.; Thayumanavan, S.; Levina, G. *J. Opt. Soc. Am. B* **2001**, *18*, 1846.
(16) Robinson, B.; Dalton, L. *J. Phys. Chem. A* **2000**, *104*, 4785.
(17) Shen, Y. R. *The Principles of Nonlinear Optics*; John Wiley & Sons: New York, 1984.
(18) Pereverzev, Y.; Prezhdo, O.; Dalton, L. *J. Chem. Phys.* **2002**, *117*, 3354.
(19) Pereverzev, Y.; Prezhdo, O.; Dalton, L. *ChemPhysChem* **2004**, *5*, 1821.
(20) Singer, K.; Kuzyk, M.; Sohn, J. *J. Opt. Soc. Am. B* **1987**, *4*, 968.
(21) van der Vorst, C.; Picken, S. *J. Opt. Soc. Am. B* **1990**, *7*, 320.
(22) Ghebremichael, F.; Kuzyk, M.; Singer, K.; Andrews, T. *J. Opt. Soc. Am. B* **1998**, *15*, 2294.
(23) Kim, W.; Hayden, L. *J. Chem. Phys.* **1999**, *111*, 5212.
(24) Makowska-Janusik, M.; Reis, H.; Papadopoulos, M.; Economou, I.; Zacharopoulos, N. *J. Phys. Chem. B* **2004**, *108*, 588.
(25) Ha, T.; Glass, J.; Enderle, T.; Chemla, D.; Weiss, S. *Phys. Rev. Lett.* **1998**, *80*, 2093.
(26) Ha, T.; Laurence, T.; Chemla, D.; Weiss, S. *J. Phys. Chem. B* **1999**, *103*, 6839.
(27) Deschenes, L.; Vanden Bout, D. *J. Phys. Chem. B* **2001**, *105*, 11978.
(28) Deschenes, L.; Vanden Bout, D. *Science* **2001**, *292*, 255.
(29) Deschenes, L.; Vanden Bout, D. *J. Chem. Phys.* **2002**, *116*, 5850.
(30) Viteri, C.; Gilliland, J.; Yip, W. *J. Am. Chem. Soc.* **2003**, *125*, 1980.
(31) Tomczak, N.; Vallee, R.; van Dijk, E.; Garcia-Parajo, M.; Kuipers, L.; van Hulst, N.; Vancso, G. *Eur. Polym. J.* **2004**, *40*, 1001.
(32) Fourkas, J. *Opt. Lett.* **2001**, *26*, 211.
(33) Bartko, A.; Dickson, R. *J. Phys. Chem. B* **1999**, *103*, 11237.
(34) Bartko, A.; Xu, K.; Dickson, R. *Phys. Rev. Lett.* **2002**, *89*, 026101.
(35) Hohlbein, J.; Hubner, C. *Appl. Phys. Lett.* **2005**, *86*, 121106.
(36) Chung, I.; Shimizu, K.; Bawendi, M. *Proc. Natl. Acad. Sci. U.S.A.* **2003**, *100*, 405.
(37) Moylan, C.; Ermer, S.; Lovejoy, S.; McComb, I.; Leung, D.; Wortmann, R.; Krdmer, P.; Twieg, R. *J. Am. Chem. Soc.* **1996**, *118*, 12950.
(38) Bondarev, S.; Knyukshto, V.; Stepuro, V.; Stupak, A.; Turban, A. *J. Appl. Spectrosc.* **2004**, *71*, 194.
(39) Juang, C.; Finzi, L.; Bustamante, C. *Rev. Sci. Instrum.* **1988**, *59*, 2399.
(40) Axelrod, D. *Biophys. J.* **1979**, *26*, 557.
(41) Ediger, M. *Annu. Rev. Phys. Chem.* **2000**, *51*, 99.
(42) Inoue, T.; Cicerone, M.; Ediger, M. *Macromolecules* **1995**, *28*, 3425.
(43) Wang, L.; Richert, R. *J. Chem. Phys.* **2004**, *120*, 11082.
(44) Sanchis, A.; Prolongo, M.; Masegosa, R.; Rubio, R. *Macromolecules* **1995**, *28*, 2693.
(45) Dureiko, R.; Schuele, D.; Singer, K. *J. Opt. Soc. Am. B* **1998**, *15*, 338.
(46) Yip, W.; Hu, D.; Yu, J.; Vanden Bout, D.; Barbara, P. *J. Phys. Chem. A* **1998**, *102*, 7564.
(47) Stahelin, M.; Walsh, C.; Burland, D.; Miller, R.; Twieg, R.; Volksen, W. *J. Appl. Phys.* **1993**, *73*, 8471.
(48) Hampsch, H.; Yang, J.; Wong, G.; Torkelson, J. *Macromolecules* **1990**, *23*, 3640.
(49) Le Floc'h, V.; Brasselet, S.; Roch, J.; Zyss, J. *J. Phys. Chem. B* **2003**, *107*, 12403.
(50) Chen, A.; Chuyanov, V.; Marti-Carrera, F.; Garner, S.; Steier, W.; Chen, J.; Sun, S.; Dalton, L. *Opt. Eng.* **2000**, *39*, 1507.